Diamond photovoltaic radiation sensor using *pn* junction

Takehiro Shimaoka,[1,a)] Satoshi Koizumi,[1] and Manobu M. Tanaka[2]
[1]*National Institute for Materials Science (NIMS), Tsukuba, Ibaraki 305-0044, Japan*
[2]*High Energy Accelerator Research Organization, Tsukuba, Ibaraki 305-0801, Japan*

(Received 11 April 2018; accepted 3 August 2018; published online 29 August 2018)

Because of its heat resistance and radiation hardness, diamond is a suitable semiconductor material for use in radiation sensors operating under harsh environments. To date, diamond radiation sensor designs have been constrained to Metal–Insulator–Metal structures. Instead of this structure, the *pn* junction offers several advantages for radiation sensors such as high built-in bias, electric field control, and depletion layer thickness control through doping profile design. We formed diamond *pn* diodes with ideal electric properties. A large built-in bias of 4.7 eV was obtained. The diode represented less than 10^{-11} A of low leakage current up to nearly 1 MV/cm of a high electric field. We detected alpha particles at zero-bias voltage using the *pn* diode, which opens the possibility of realizing compact radiation sensors. *Published by AIP Publishing.* https://doi.org/10.1063/1.5034413

Diamond *pn* diodes[1] have been studied for use as deep ultra violet (DUV) light emitting diodes[2,3] and DUV sensors[4] and have been investigated for power electronics applications.[5] The diode is presumably applicable for radiation sensors operating in harsh environments such as nuclear reactors and accelerators because diamond has radiation hardness[6] and heat resistance[7] attributable to its 5.5 eV wide bandgap.

The Metal–Insulator–Metal (MIM) structure has been widely used for diamond radiation sensors. In this configuration, high-purity diamond plates are sandwiched between two electrodes. The sensor requires an electric field of several kV/cm to 10 kV/cm to saturate the charge collection efficiency (CCE). More recently, new diamond radiation detectors such as membrane detectors[8] and MIS structures[9] have been invented. One benefit of using these detectors is that they achieve excellent CCE with low bias voltage by reduction of the drift length of the charge carrier.

The diamond *pn* junction is suitable for this purpose because it has 4.5 eV of large built-in potential (V_{bi}). The V_{bi} is more than twice those of typical diamond Schottky barrier diodes. Large V_{bi} can improve charge collection properties: it is expected to form a field sufficient to transport charges created by radiation when the drift layer thickness is several micrometers. Small sensors without a bias voltage power supply can be realized using a *pn* junction. Such compact and durable diamond radiation sensors can be used for the nuclear decommissioning work, with its expected exposure to extreme radiation.

The *pn* junction also presents the possibility of adjusting sensitivity against radiation in terms of the variation of the energy range by the doping profile design. It can form an extremely thin drift layer, which is difficult to form merely by etching of bulk diamond. Control of the drift layer thickness is important for energy discrimination of charged-particle measurements under high energy gamma or x-ray flux. This control can be useful for measurements such as neutral particle measurements of nuclear fusion diagnostics.[10] Control of sensitivity against radiation provides a wide dynamic range of measurements against gamma and X-ray radiation doses.

In addition to sensor operation, the *pn* junction can improve the energy conversion efficiency of radiation batteries. Recently, some research groups have reported betavoltaic cells and photovoltaic radiation sensors produced using diamond Schottky diodes.[11,12] Because *pn* junctions have larger built-in bias, diamond *pn* junctions present some potential to improve photovoltaic efficiency.

For this study, this report describes photovoltaic operation of the diamond *pn* diode and charge transport characteristics of a 1 μm thin drift layer up to nearly 1 MV/cm of the high field. We formed pseudo-vertical diamond *pn* diodes. A schematic drawing of the diode structure is portrayed in Fig. 1. Homoepitaxial p^+, n^-, and n^+-layers were grown on a {111} HPHT type Ib single-crystal diamond substrate using microwave-assisted plasma chemical vapor deposition. A mesa structure was formed using reactive ion etching with oxygen gas. The mesa diameter was Ø240 μm. Ohmic contacts were formed by electron beam deposition of Ti/Mo/Au both on the mesa structure of the n^+-layer and on the p^+-layer. The contact diameter was Ø150 μm. Doping concentrations

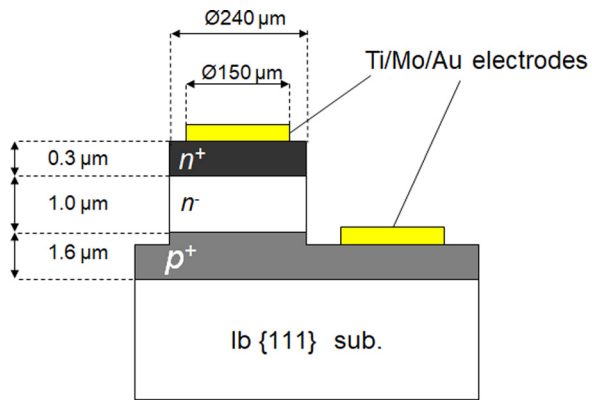

FIG. 1. Schematic drawing of the diamond *pn* diode. Homoepitaxial p^+, n^-, and n^+-layers were grown on the {111} HPHT type Ib single-crystal diamond substrate using microwave-assisted plasma chemical vapor deposition. The doping concentrations of p^+, n^-, and n^+ layers confirmed by SIMS were [B] 2×10^{19} cm^{-3}, [P] 1×10^{16} cm^{-3}, and [P] 1×10^{20} cm^{-3}, respectively.

a)Author to whom correspondence should be addressed: SHIMAOKA. Takehiro@nims.go.jp

and the thicknesses of the respective layers were confirmed using secondary mass ion spectrometry (SIMS). The doping concentrations of p^+, n^-, and n^+-layers were [B] 2×10^{19} cm^{-3}, [P] 1×10^{16} cm^{-3}, and [P] 1×10^{20} cm^{-3}, respectively. The respective thicknesses of p^+, n^-, and n^+-layers were 1.6 μm, 1.0 μm, and 0.3 μm.

We used a microprobe system to assess *I–V* and *C–V* characteristics of the diode. Both measurements were done under high vacuum. The base pressure of the vacuum chamber was approximately 10^{-11} Torr. A source measure unit (E5280B; Agilent Technologies, Inc.) and an inductance-capacitance-resistance (LCR) meter (4284A; Agilent Technologies, Inc.) were used for the measurements. An applied frequency was 500 Hz in the *C-V* measurement. Furthermore, we measured the alpha-particle induced charge distribution of the diamond *pn* diode. An experimental setup is depicted in Fig. 2. The contacts were connected using Au wire bonding to the SMA coaxial connector and Al housing. Alpha particles from the ^{241}Am radioactive source were injected from the n^+ contact side. Because the alpha particle energy is 5.486 MeV and because their extinction range in diamond is 13 μm, alpha particles traverse the whole depletion layer of the diamond *pn* diode. Measurements were taken under low vacuum: sub-Pascal.

We define the charge collection efficiency (CCE) of the *pn* diode as

$$CCE(\%) = \frac{Q_{collected}}{Q_{induced}} \times 100, \tag{1}$$

$$Q_{induced} = qN_{EHP} = \frac{q \times LET \times w}{W}. \tag{2}$$

CCE is expressed as the percent of collected charge ($Q_{collected}$) to induced charge ($Q_{induced}$) in the depletion layer. Here, q, N_{EHP}, and W represent the elementary charge, the number of created electron-hole pairs, and the pair-creation energy, respectively. LET stands for the linear energy transfer of alpha particles. Using the TRIM code, LET was estimated as 270 keV/μm.[13] w represents the depletion layer thickness. From SIMS profiles, w of the full depletion width in the *pn* diode was deduced as 1 μm. A silicon PIN photodiode (S3590; Hamamatsu Photonics KK) was used for calibration of the induced charge. The average pair creation energies W of diamond and silicon are 12.8 eV and 3.62 eV, respectively.[14] Reverse bias was applied during measurements. A charge-sensitive preamplifier (1442A; C AEN S.p.A.), a spectroscopy amplifier (968d; CAEN S.p.A.), and a multichannel analyzer (8000D; Amptek, Inc.) were used for pulse height analysis.

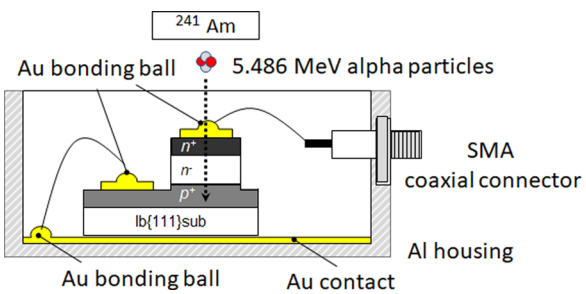

FIG. 2. Experimental setup of the alpha-particle induced charge distribution measurement. Alpha particles from the ^{241}Am radioactive source were injected from the n^+ contact side. 5.486 MeV alpha particles traverse the whole depletion layer of the diamond *pn* diode.

Figure 3 presents *I–V* characteristics of the *pn* diode. The rectification ratio was 10^{10} at ± 10 V. The diode represented less than 10^{-11} A of low leakage current up to 100 V. The applied field was estimated as 1 MV/cm of the high electric field. The relevant *C–V* and $1/C^2$–*V* curves are presented in Fig. 4. We evaluated a net positively charged ionization impurity N_D-N_A and built-in potential V_{bi} using the following equation:

$$N_D - N_A = \frac{2}{q\varepsilon\varepsilon_0 A^2} \frac{1}{d(1/C^2)/dV}, \tag{3}$$

$$V - V_{bi} = \frac{q\varepsilon\varepsilon_0 (N_D - N_A)}{2A^2} \frac{1}{C^2}. \tag{4}$$

In Eqs. (3) and (4), q denotes the elementary charge, ε stands for the permittivity of diamond, ε_0 stands for the permittivity of vacuum, and A is the diode area. The linear region was used for the fitting because the curve of $1/C^2$–*V* profiles reflects the gradient of the doping concentration. N_D-N_A was 2.9×10^{15} cm^{-3}. V_{bi} was deduced as 4.7 V. Saturation of the $1/C^2$–*V* profiles showed full depletion of the n^- layer at approximately 8 V of reverse bias voltage. The depletion layer thickness deduced from capacitance was 1.1 μm, which showed good agreement with the drift layer thickness estimated from SIMS. 10% of the deference in the depletion layer may be attributed to the dispersion effect of the deep level of the P donor. A portion of charges may not be unable to contribute to the net space charge.[15]

Figure 5 presents the induced charge distribution of the *pn* diode at zero bias voltage. The *pn* diode can detect alpha particles without external bias voltage. Two peaks of induced charge are shown. The peak of the lower energy side was the distribution of the induced charge formed by alpha particles injected directly into the n^+-layer of the diode. CCE was 40%. The energy resolution of the peak was 30%. The peak of the higher energy side was presumed to reflect the induced charge created by alpha particles that traverse the Au wire

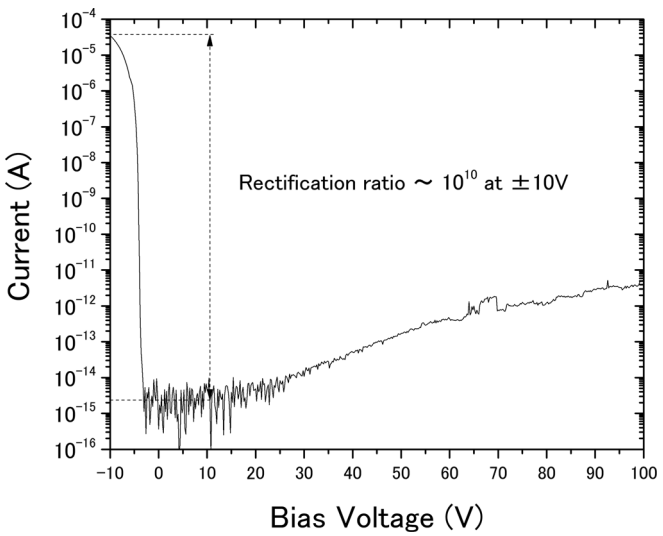

FIG. 3. *I–V* characteristics of the *pn* diode. The diode showed excellent diode properties. The rectification ratio was 10^{10} at ± 10 V. The diode represented less than 10^{-11} A of low leakage current up to 100 V.

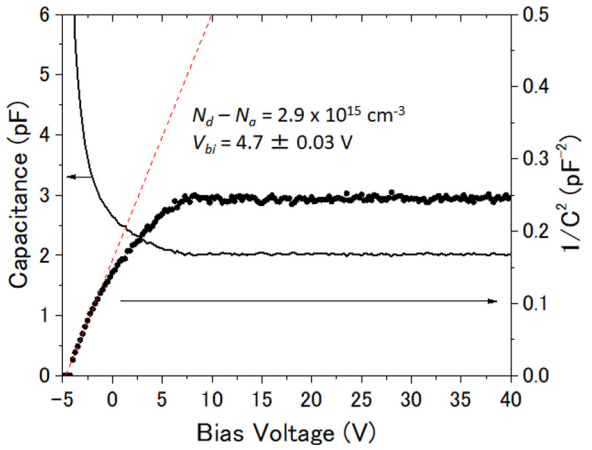

FIG. 4. C–V and $1/C^2$–V curves of the pn diode. The dashed line shows fitting by Eqs. (3) and (4). Net positive charge density and built-in bias were 2.9×10^{15} cm^{-3} and 4.7 ± 0.03 V, respectively. Saturation of $1/C^2$–V profiles showed full depletion of the n^- layer at approximately 8 V of reverse bias voltage.

bonding ball. Energy loss by the contact and the wet area of the Au bonding ball might increase the LET of alpha particles.

The reverse bias dependence of the induced charge is presented in Fig. 6, in which the error bar shows the full width at half maximum of the collected charge distribution. The left side of the vertical axis shows the CCE in the depletion layer. The right side of the vertical axis represents the collected charge. LET in diamond was 270 keV from the surface to 1 μm. Here, 3.4 fC is equivalent to nearly 100% of CCE. The saturated collected charge showed 30% of larger CCE. Diffusion of the charge carrier from n^+ and p^+ layers might contribute to some of the detected charges. Alpha particles injected with an inclined angle might also increase the induced charge by the increase in the traversal distance of alpha particles in the depletion layer. More than 10 times of the field strength was necessary to saturate CCE compared to the field strength of the MIM structure. The average field

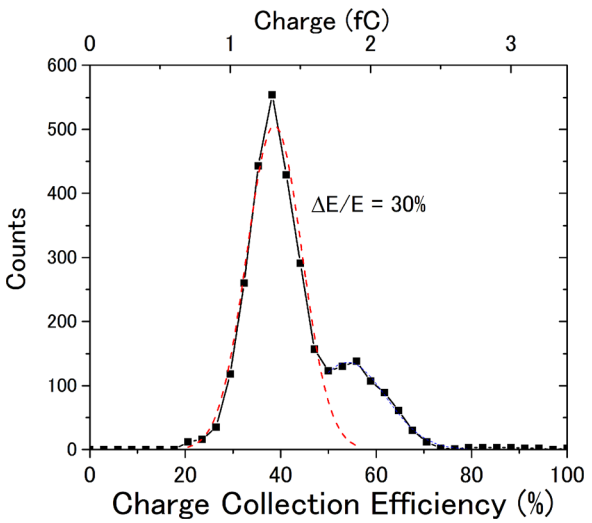

FIG. 5. Induced charge distribution of the pn diode at zero bias voltage. The pn diode can detect alpha particles without external bias voltage. The dashed line shows Gaussian fitting. Charge collection efficiency was approximately 40%. Energy resolution of 30% was obtained. A peak of the higher energy side was presumed to reflect the induced charge created by alpha particles that traverse the Au wire-bonding ball.

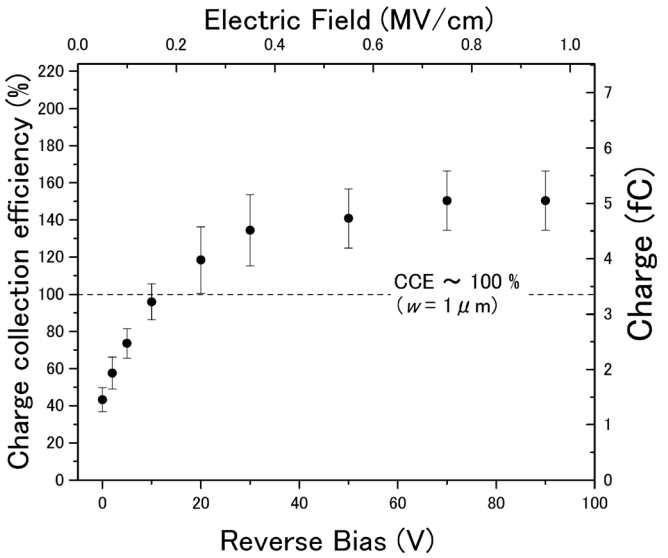

FIG. 6. Reverse bias dependence of induced charge. The error bar represents the full width at half maximum. More than 30 V of reverse bias voltage was necessary to saturate the collected charge, which is three times higher bias voltage than the voltage for full depletion of the n^- layer. Diffusion of the charge carrier from n^+ and p^+ layer might contribute to the collected charge, which exceeds 100% of CCE.

strength estimated from the planar structure ($E = V_R/w$) at 30 V was approximately 0.3 MV/cm. Our sample showed full depletion of the drift layer at 8 V of reverse bias voltage. An increase in the depletion layer thickness does not contribute to an increase in CCE when the reverse bias voltage is greater than 8 V.

Two factors might degrade charge transport. First is the drift layer crystallinity. The impurity level of the thick crystal is less than 10^{15} cm^{-3}. By contrast, our sample used the n-layer as a drift layer. The layer includes 10^{16} cm^{-3} of phosphorous. An increased impurity level decreases the carrier lifetime.

The second factor is polarization effects, which might enhance the recombination of charge carriers. For that reason, the pn diode with a thin drift layer presumably requires a larger electric field to saturate collected charges than that of a thick drift layer. Figure 7 presents the ratio of the collected charge to the saturated charge in the drift layer as a function of the electric field. Datasets of thick and thin diamond detectors have been presented elsewhere.[16,17] A thin drift layer ($w < d$) shows poor charge collection properties, which might result from transient degradation of field strength by space charge formation.[17,18] In cases where the depletion layer width w is sufficiently large for the range of charged particles d, the e–h pair mainly formed near the top electrode. The electric field of the remainder of the drift layer might not be affected by the space charge. In the case of $w < d$, the e–h pair formed throughout the depletion layer. The space charge might decrease the electric field strength.

To improve the charge collection property of the pn diode, the drift layer impurity level should be decreased to less than 10^{15} cm^{-3}. The drift layer thickness should also be optimized by the range of charged particles.

We evaluated the bias dependency of the induced charge up to 90 V. The estimated average electric field was 0.9 MV/cm. Skukan *et al.* reported charge multiplication using a membrane diamond detector.[17] They report charge multiplication

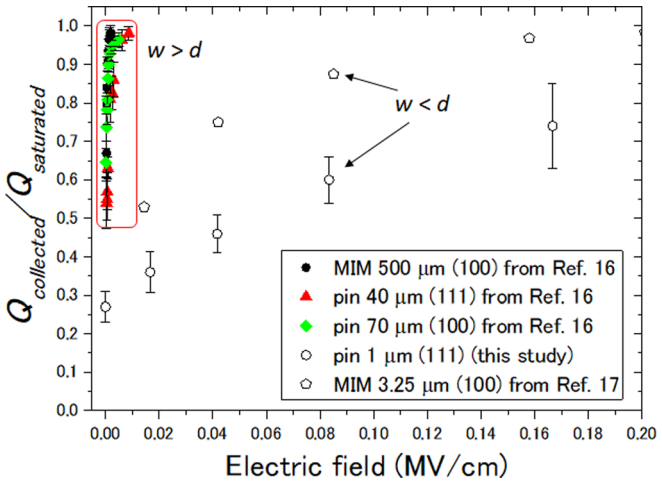

FIG. 7. Ratio of the collected charge to the saturated charge in the drift layer as a function of the electric field. w represents the drift layer thickness. d stands for the range of alpha-particles in diamond. The thin drift layer ($w < d$) shows poor charge collection properties compared to that of thick drift layer ($w \gg d$), presumably because of transient degradation of the field strength by space charge formation.

under sub-MV/cm to 2 MV/cm electric fields. In our case however, we were unable to conclude that the charge is multiplied in the layer because nonlinear multiplication was not observed clearly. Even higher fields must be used to confirm avalanche multiplication in *pn* junctions.

In conclusion, we formed a diamond *pn* diode with ideal electrical properties. The diode, which showed 4.7 eV of ideal built-in bias, can detect alpha particles at zero-bias voltage. The electric field for the saturation of collected charge required 0.3 MV/cm. Polarization effects through the depletion layer might degrade the electric field and adversely affect the charge transport characteristics.

This study was supported by the Cross-ministerial Strategic Innovation Promotion Program (SIP), P14029, and a JSPS Grant for Young Scientists (B) No. 17K14914.

[1]S. Koizumi, K. Watanabe, M. Hasegawa, and H. Kanda, Science **292**, 1899–1901 (2001).
[2]T. Makino, K. Yoshino, N. Sakai, K. Uchida, S. Koizumi, H. Kato, D. Takeuchi, M. Ogura, K. Ohyama, T. Matsumoto, H. Okushi, and S. Yamasaki, Appl. Phys. Lett. **99**, 061110 (2011).
[3]T. Makino, S. Tanimoto, Y. Hayashi, H. Kato, N. Tokuda, M. Ogura, D. Takeuchi, K. Oyama, H. Ohashi, H. Okushi, and S. Yamasaki, Appl. Phys. Lett. **94**, 262101 (2009).
[4]A. BenMoussa, J. F. Hochedez, U. Schuhle, W. Schmutz, K. Haenen, Y. Stockman, A. Soltani, F. Scholze, U. Kroth, V. Mortet, A. Theissen, C. Laubis, M. Richter, S. Koller, J.-M. Defise, and S. Koizumi, Diamond Relat. Mater. **15**, 802 (2006).
[5]M. Suzuki, T. Sakai, T. Makino, H. Kato, D. Takeuchi, M. Ogura, H. Ohkushi, and S. Yamasaki, Phys. Status Solidi **210**, 2035 (2013).
[6]A. Alekseyev, V. Amosov, Y. Kaschuck, A. Krasilnikov, D. Portnov, and S. Tugarinov, Nucl. Instrum. Methods Phys. Res., Sect. A **476**, 516 (2002).
[7]M. Tsubota, J. H. Kaneko, D. Miyazaki, T. Shimaoka, K. Ueno, T. Tadokoro, A. Chayahara, H. Watanabe, Y. Kato, S. Shikata, and H. Kuwabara, Nucl. Instrum. Methods Phys. Res., Sect. A **789**, 50 (2015).
[8]M. Pomorski, B. Caylar, and P. Bergonzo, Appl. Phys. Lett. **103**, 112106 (2013).
[9]S. Almaviva, M. Marinelli, E. Milani, G. Prestopino, A. Tucciarone, C. Verona, G. Verona-Rinati, M. Angerlone, M. Pillon, I. Dolbnya, K. Sawhney, and N. Tartoni, J. Appl. Phys. **107**, 014511 (2010).
[10]A. V. Krasilnikov, S. S. Medley, N. N. Gorelenkov, R. V. Bundy, O. V. Ignatyev, Y. A. Kachunk, M. P. Petrov, and A. L. Roquemore, Rev. Sci. Instrum. **70**, 1107 (1999).
[11]C. Delfaure, M. Pomorski, J. de Sanoit, P. Bergonzo, and S. Saada, Appl. Phys. Lett. **108**, 252105 (2016).
[12]S. Almaviva, M. Marinelli, E. Milani, A. Tucciarone, G. V. Rinati, R. Consorti, A. Petrucci, F. De Notaristefani, and I. Ciancaglioni, Nucl. Instrum. Methods Phys. Res., Sect. A **594**, 273 (2008).
[13]J. F. Ziegler, J. P. Biersack, and M. D. Ziegler, *The Stopping and Range of Ions in Solids* (Pergamon Press, New York, USA, 1985).
[14]M. Pomorski, E. Berdermann, W. de Boer, A. Furgeri, C. Sander, and J. Morse, Diamond Relat. Mater. **16**, 1066 (2007).
[15]M. Suzuki, S. Koizumi, M. Katagiri, T. Ono, N. Sakuma, H. Yoshida, T. Sakai, and S. Uchikoga, Phys. Status Solidi A **203**, 3128 (2006).
[16]T. Shimaoka, D. Kuwabara, A. Hara, T. Makino, M. Tanaka, and S. Koizumi, Appl. Phys. Lett. **110**, 212104 (2017).
[17]N. Skukan, V. Grilj, I. Sudic, M. Pomorski, W. Kada, T. Makino, Y. Kambayashi, Y. Andoh, S. Onoda, S. Sato, T. Ohshima, T. Kamiya, and M. Jaksic, Appl. Phys. Lett. **109**, 043502 (2016).
[18]S. Sato, T. Makino, T. Ohsima, T. Kamiya, W. Kada, O. Hanaizumi, V. Grilj, N. Skukan, M. Pomorski, and G. Vizkelethy, Diamond Relat. Mater. **75**, 161 (2017).